



ELSEVIER

Available online at www.sciencedirect.com



Fluid Dynamics Research 40 (2008) 497–509

FLUID DYNAMICS
RESEARCH

Phase-Field simulation of small capillary-number two-phase flow in a microtube

Qunwu He*, Nobuhide Kasagi

Department of Mechanical Engineering, The University of Tokyo, Hongo 7-3-1, Bunkyo-ku, Tokyo 113-8656, Japan

Received 19 November 2007; received in revised form 22 January 2008; accepted 22 January 2008

Available online 12 May 2008

Communicated by A. Prosperetti

Abstract

Accurate calculation of surface tension force is critically important for numerical simulation of gas–liquid two-phase flows at small capillary number. It is well known that the errors in the surface tension calculation would cause considerable parasitic flow with conventional continuum surface force method. In the present simulation, Phase-Field method is employed to capture local two-phase interface. The surface tension force is represented by a chemical potential gradient. The numerical results show that the chemical potential formulation of surface tension force can reduce the magnitude of parasitic flow to the level of truncation error. This is because exchange between kinetic and surface energy is appropriately calculated. The method is applied to the simulations of air–water two-phase bubbly and slug flows in a microtube of 600 μm . The Reynolds numbers are 60–200, and the capillary number is $O(10^{-3})$. The simulated gas bubble shape and two-phase flow patterns are in good agreement with experimental results. The pressure drop, represented by Lockhart–Martinelli correlation, is found larger than that proposed for tubes in millimeter.

© 2008 The Japan Society of Fluid Mechanics and Elsevier B.V. All rights reserved.

Keywords: Two-phase flow; Capillary number; Parasitic flow; Phase-Field method

1. Introduction

Multiphase microfluidic is a rapidly expanding field due to its potential applications such as micro heat exchangers and Lab-on-a-chip. Although extensive experimental studies have been reported on gas–liquid

* Corresponding author.

E-mail address: qwhe@thtlab.t.u-tokyo.ac.jp (Q. He).

two-phase flow and boiling heat transfer in mini and micro conduits, there seems to still exist considerable discrepancies, largely due to the difficulties in experimental setup and measurements (Kandlikar, 2002). To understand the detailed mechanism of two-phase flow in micro conduits, advanced numerical simulation is indispensable.

A relatively new method, the so-called Phase-Field method, is getting more popular, because it provides a new insight in describing the interface. It is based on fluid free energy instead of force (Anderson et al., 1998). The advantages of this approach are:

- (1) Topology changes without difficulties; interfaces can either merge or break up, while no extra coding is required.
- (2) The composition field has physical meanings not only on the interface but also in the bulk phase. Therefore, this method can be applied to many physical phase states such as miscible, immiscible, and partially miscible ones.
- (3) The method is able to simulate contact line motion.

To represent surface tension force, the continuum surface force (CSF) model, which is proposed by Brackbill et al. (1992), has been widely used. In the CSF model, the surface tension effect is treated as a body force. It is distributed within a transition region of finite thickness at the interface, and given by

$$F_S = -\sigma \int_S \kappa \mathbf{n} \delta(\mathbf{x} - \mathbf{x}_S) dS, \quad (1)$$

where σ is the surface tension coefficient, κ is the interface curvature, \mathbf{n} is the unit normal to the surface in the outward direction, $\delta(\mathbf{x} - \mathbf{x}_S)$ is the smoothed Dirac delta function, and \mathbf{x}_S is the location of interface. This continuum treatment of the discontinuous change at the interface eases the implementation of the surface tension effect.

In problems with complex topological changes, the CSF model is superior to the conventional methods in robustness and versatility. However, it is found that the CSF model generates vortex-like flows, referred to as spurious currents or parasitic flow in the literature, in the neighborhood of the interface (Lafaurie et al., 1994). For two-phase flow in micro conduits, capillary effects and other associated phenomena dominate due to the large curvature of the interface between phases. The generated parasitic flow may destroy the interface and even cause disruptive instabilities.

Continuous efforts have been made in recent studies to reduce the spurious currents and improve the modeling of surface tension force. Popinet and Zaleski (1999) improved the pressure gradient calculation by a pressure gradient correction procedure in their front-tracking method. Based on the volume-of-fluid (VOF) method, Meier et al. (2002) used an empirical formula obtained from the database generated and stored to determine interface curvatures. It was found that the choice of density at the interfacial cells significantly affected the spurious currents. Shirani et al. (2005) attempted to remedy this issue by multiplying the body force by a factor, H , which denoted the area of a cell face in contact with the heavier liquid. In more recent work, Tong and Wang (2007) proposed a pressure boundary method. The surface tension force is incorporated into the Navier–Stokes equation via a pressure gradient, while the free surface is tracked by a coupled level-set and VOF method. It is shown that the spurious currents are greatly reduced by this method with the sharp pressure boundary condition preserved.

While improvements to the surface tension model have alleviated the spurious current, the inherent problem resulting from the local surface tension force representation remains unresolved. Jamet et al.

(2002) developed a promising approach, which can completely eliminate the parasitic currents. They concluded that the essential requirement for the elimination of the parasitic currents was energy conservation. However this approach is only applicable within the framework of the second-gradient method, where the fluids are compressible.

As an extension of the work of Jamet et al. (2002), the Phase-Field method is used to simulate an air–water two-phase system in the present work. The formulation of surface tension by CSF and chemical potential (CP) will be adopted and compared. The mechanism of the CP method will be analyzed. This method is then applied to more realistic conditions, i.e., bubbly and slug flow in a microtube.

2. Numerical methods

2.1. Phase-Field method

The Phase-Field method is a kind of diffuse-interface models of incompressible, immiscible two-phase flow (Anderson et al., 1998). In this method, an order parameter F is introduced. It is a mass fraction of one of two phases. The concentration F is governed by the so-called Cahn–Hilliard equation given as

$$\frac{\partial F}{\partial t} + (\mathbf{u} \cdot \nabla)F = \nabla \cdot (M(F)\nabla\mu), \quad (2)$$

$$\mu = \phi'(F) - \varepsilon^2 \nabla^2 F, \quad (3)$$

where $M(F)$, $\phi(F)$ and ε are the mobility, bulk energy density and interface thickness parameter, respectively. For simplicity, the mobility $M(F)$ is assumed as a constant in the present study. The bulk energy density $\phi(F)$ is defined as $F^2(1 - F^2)/4$, which is a double-well positive function and has two minima corresponding to the two stable phases. The immiscibility of fluid components has also been modeled thereby. It can be shown that the classical Navier–Stokes equations and pressure jump conditions are recovered in the sharp interface limit of $\varepsilon \rightarrow 0$ (Anderson et al., 1998). The chemical potential, μ , is the rate of change of free energy with respect to F . Therefore, the equilibrium interface profiles are the solutions when μ is constant.

For immiscible and incompressible two-phase flow, the governing equations of velocity can be written as

$$\nabla \cdot \mathbf{u} = 0, \quad (4)$$

$$\frac{\partial(\rho\mathbf{u})}{\partial t} + \mathbf{u} \cdot \nabla(\rho\mathbf{u}) = -\nabla p + \nabla \cdot [\eta(\nabla\mathbf{u} + \nabla\mathbf{u}^T)] + \mathbf{F}_S + \mathbf{g}, \quad (5)$$

where ρ and η denote the density and viscosity, respectively, and are determined according to the position of interface. The terms of \mathbf{F}_S and \mathbf{g} in Eq. (5) represent the surface tension and gravitational force, respectively.

According to the CSF formulation, the surface tension force \mathbf{F}_S is converted to a form of volume force and the resulting force is proportional to the product of the interface gradient and the surface curvature, i.e.,

$$\mathbf{F}_S = -\sigma\kappa(\phi)\delta(\phi)\nabla\phi, \quad (6)$$

in which ϕ is the distance function and the volume fraction for the level-set and VOF method, respectively. When applying to the Phase-Field method, Kim (2005) proposed a surface tension force formulation by taking a form similar to Eq. (6),

$$F_S = -\sigma \nabla \cdot \left(\frac{\nabla F}{|\nabla F|} \right) \varepsilon \alpha |\nabla F|^2 \frac{\nabla F}{|\nabla F|}, \quad (7)$$

where $\nabla \cdot (\nabla F/|\nabla F|)$, $\varepsilon \alpha |\nabla F|^2$, and $\nabla F/|\nabla F|$ correspond to $\kappa(\phi)$, $\delta(\phi)$, and $\nabla \phi$ in Eq. (6), respectively.

On the other hand, based on the fluid free energy, Jacqmin (1999) proposed the CP formulation of surface tension force. It is based on the assumption that the change in kinetic energy is always opposite to the change in free energy and reads

$$F_S = -F \nabla \mu. \quad (8)$$

Jacqmin (1999) has shown that the forms of surface tension of Eqs. (7) and (8) are deducible from each other.

2.2. Non-dimensionlization and discretization of surface tension force

We define the dimensionless variables as

$$x' = \frac{x}{L_c}, \quad \mathbf{u}' = \frac{\mathbf{u}}{U_c}, \quad t' = \frac{t U_c}{L_c}, \quad p' = \frac{p}{\rho_c U_c^2}, \quad (9)$$

where L_c is the characteristic length, which is taken to be the radius of tube R in the present study, U_c is the characteristic velocity, and ρ_c is the characteristic density defined as that of water. Dropping the primes, the dimensionless equations are written as

$$\nabla \cdot \mathbf{u} = 0, \quad (10)$$

$$\frac{\partial(\rho \mathbf{u})}{\partial t} + \mathbf{u} \cdot \nabla(\rho \mathbf{u}) = -\nabla p + \frac{1}{Re} \nabla \cdot [\eta(\nabla \mathbf{u} + \nabla \mathbf{u}^T)] + F_S + \frac{\mathbf{g}}{Fr}, \quad (11)$$

$$\frac{\partial F}{\partial t} + (\mathbf{u} \cdot \nabla) F = \frac{1}{Pe} \nabla^2 \mu, \quad (12)$$

$$\mu = \varphi'(F) - Cn^2 \nabla^2 F. \quad (13)$$

The dimensionless physical parameters are defined as

$$Re = \frac{\rho_c U_c L_c}{\eta_c}, \quad Fr = \frac{U_c^2}{gL_c}, \quad Pe = \frac{U_c L_c}{M_c \mu_c}, \quad Cn = \frac{\varepsilon}{L_c}. \quad (14)$$

The choice of Cn is influenced by numerical accuracy, efficiency and stability (Jacqmin, 1999). For the CSF model, F_S in Eq. (11) becomes

$$F_S = -\frac{\sigma \gamma \varepsilon}{We} \nabla \cdot \left(\frac{\nabla F}{|\nabla F|} \right) |\nabla F|^2 \frac{\nabla F}{|\nabla F|}, \quad (15)$$

and correspondingly, for the CP model,

$$F_S = -\frac{\sigma\gamma}{\varepsilon We} F \nabla \mu, \quad (16)$$

where the Weber number is defined as $We = \rho_c U_c^2 L_c / \sigma$. The concentration field F should be locally in equilibrium during evolution. To match the surface tension of the sharp interface model, it must satisfy

$$\varepsilon\gamma \int_{-\infty}^{\infty} (F_S^{\text{eq}}(x))^2 dx = 1. \quad (17)$$

The one-dimensional (say, along the x -direction) non-uniform solution gives the equilibrium composition profile, i.e.,

$$F^{\text{eq}}(x) = \frac{1 + \tanh(x/2\sqrt{2}\varepsilon)}{2}, \quad (18)$$

and $\gamma = 6\sqrt{2}$ as was first obtained by van der Waals.

3. Results and discussion

3.1. Validation of numerical simulation

Computations are carried out for a non-evaporating bubble rising in a liquid to validate the Phase-Field formulation and the computation code. The bubble would rise by gravity and reach a steady speed/shape due to viscous and surface tension forces. The computational domain is chosen as a cylindrical region, $6R$ in radius and $12R$ in height to avoid the effect of outer boundary conditions. A 96×192 uniform Cartesian grid is used. The Navier–Stokes equations are solved by the SMAC method. The second-order central difference scheme is used for the spatial discretization. The pressure Poisson equation is solved by the successive over-relaxation (SOR) scheme. An equally spaced staggered grid system is adopted. The Cahn–Hilliard equation is solved by the CIP (cubic-interpolated pseudo-particle) scheme, which has nearly spectral accuracy. The right-hand-side terms of Eqs. (11)–(13) are discretized by using the standard central difference scheme. For non-dimensional parameters, the experimental conditions and the steady rising velocity, reported by Hnat and Buckmaster (1976), are adopted as the characteristic length and velocity, respectively. The corresponding Re number is 9.8, We number is 7.6 and Fr number equals 0.78. Therefore, the dimensionless rising velocity expected in simulation is 1.

The simulation is started with a spherical bubble of dimensionless radius one. Fig. 1 shows time traces of bubble rising velocity and terminal bubble shapes. The velocity of steady state is 1.03 in the present simulation. Sussman et al. (1994) simulated the same flow using level-set method. Their result of bubble shape is also shown in Fig. 1(c) for comparison. The terminal velocity in their simulation is 0.98. Fairly good agreement on bubble shape and rising velocity is obvious. Therefore, the present method is capable to simulate the two-phase flow with fairly good accuracy.

3.2. Stationary bubble

Numerical experiments using the CSF and CP models are carried out. The model problem chosen is an axisymmetric gas bubble in quiescent water. As no external force acts on the bubble, its equilibrium

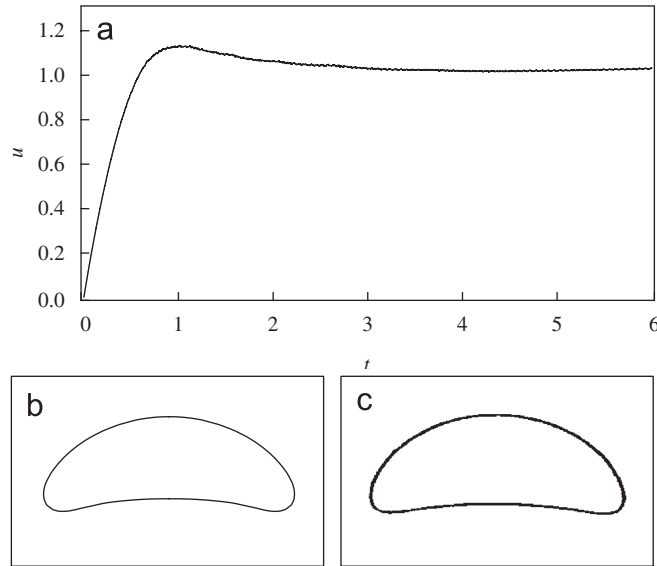


Fig. 1. Gas bubble rising in quiescent water: (a) Rising velocity; (b) bubble shape at the steady state; and (c) numerical results by Sussman et al. (1994).

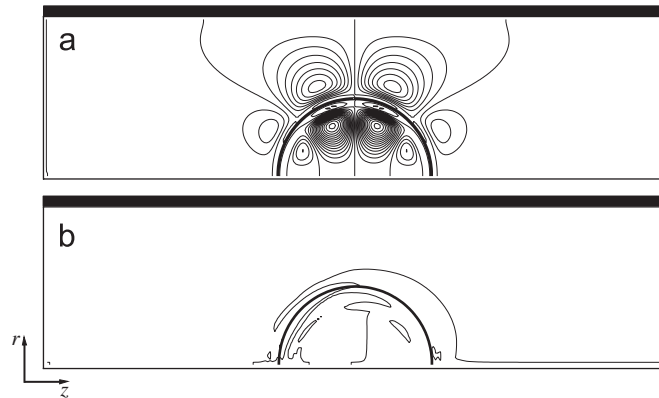


Fig. 2. Streamlines of parasitic flow for different surface tension models: (a) CSF and (b) CP.

position should be the same as its initial position and all velocity components should be zero. The maximum magnitude of parasitic current components is recorded. The computational domain is an axisymmetric three-dimensional (r, z) plane with periodic boundary condition in the streamwise direction, z , and no-slip condition at the wall. The length of period is fixed at $L_z/R = 4$.

Fig. 2 shows the streamlines of parasitic flow for different surface tension models. In this case, $Re = 100$ and $We = 0.1$, while $Ca = 0.001$. The computational cell is 64×256 , and ε is set equal to Δx . The streamlines are defined as

$$\frac{1}{r} \frac{\partial \Psi}{\partial r} = u_z - U_G, \quad \frac{1}{r} \frac{\partial \Psi}{\partial z} = -u_r, \quad (19)$$

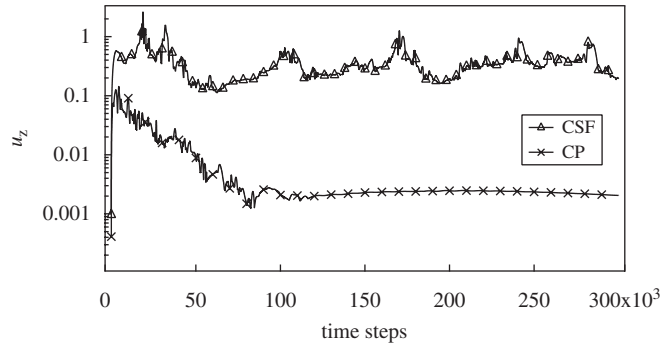


Fig. 3. Time evolution of the maximum velocity components obtained by CP and CSF models.

where the U_G is the bubble velocity. As shown in Fig. 2(a), which is obtained by the CSF method, there are clearly eight vortices near the interface. This is similar to the results by many authors (Shirani et al., 2005; Kim, 2005; Lafaurie et al., 1994). The parasitic flow originates from numerical imbalance between the surface tension force and the associated pressure gradient. Consequently, unphysical currents would inevitably be present in that region and grow when the surface tension increases. However, the parasitic flow is dramatically suppressed in the case of CP model as shown in Fig. 2(b). Initially generated discretizing error is transferred between kinetic energy and surface tension energy, and dissipated by viscosity.

Fig. 3 shows the time evolution of maximum u_z velocities with the CP and CSF models. For the CSF model, the parasitic velocity does not decrease with the time, and parasitic flow is on the order of $O(1)$. This fact indicates that, for real applications with a bulk flow, the parasitic flow would be on the same order of the bulk flow. By using the CP model, the parasitic flow rises abruptly at $t = 0$ because of numerical truncation errors in the initial force balance, but decreases exponentially thereafter by two orders of magnitude. It has been reported by Jamet et al. (2002) that it is possible to eliminate the parasitic flow to the level of computer machine accuracy. However, in the present case, because the fluids are incompressible, the parasitic flow would be on the level of truncation error. Jacqmin (1999) has demonstrated that, in discretized form, the CP model assures energy conserving. The rate of change in the free energy due to convection is the same as the rate of change in kinetic energy due to surface tension force. The initially generated energy is transferred between the kinetic energy and surface tension energy, as results in the slight movement of interface position. The exact position of interface, which is defined as $F = 0.5$ in the CP model, are shown in Fig. 4 for different time. The interface moves forward and backward alternatively due to the parasitic flow, but the magnitude of movement is still very small. In the present case, it is within $\Delta x/3$. This tiny oscillation results in the inaccuracy in the definition of interface position.

3.3. Two-phase flow in a microtube

The above numerical scheme is extended to the simulations of bubbly and slug flows in a microtube. The experiments obtained by Hayashi et al. (2007) is mainly used for comparison. The tube diameter is fixed as $600 \mu\text{m}$. Water and air at 20°C (293 K) and 1 atm are employed as working fluids, so the surface tension coefficient is 0.0728 N/m .

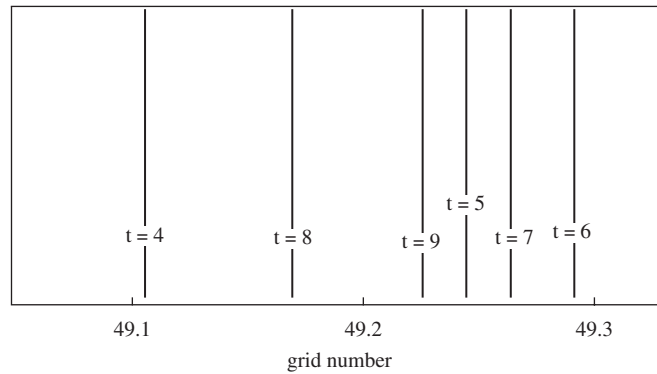


Fig. 4. Oscillation of interface position with CP model.

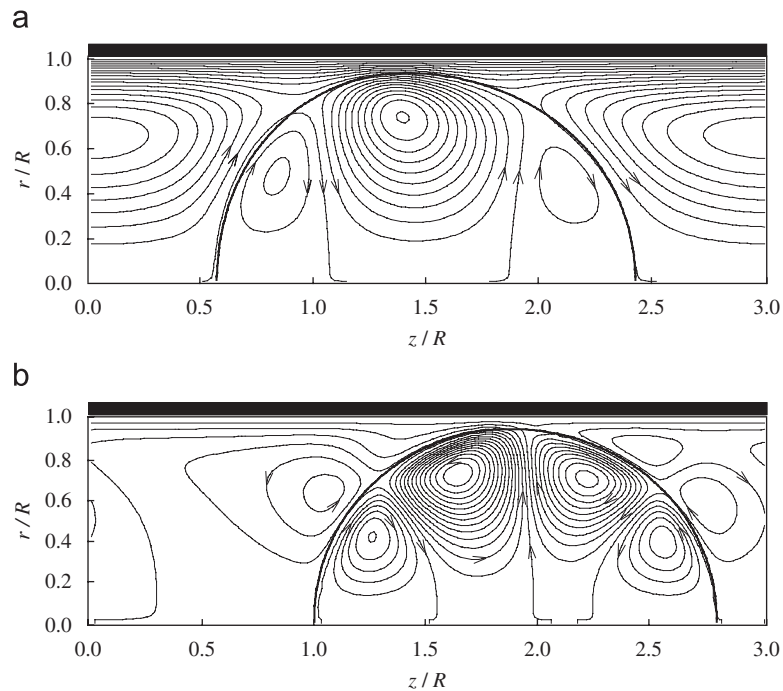


Fig. 5. Bubbly flow in a microtube simulated by CP and CSF models: (a) CP and (b) CSF.

First, simulations are performed with both CSF and CP models for the surface tension force. In accordance with the experimental conditions, $Re = 100$ and $We = 0.45$ while Fr number is ∞ due to the negligible gravity effect. Fig. 5 shows the simulated streamlines, which are calculated in the frame moving with bubble. In Fig. 5(a), the calculated streamlines are steady, and an anti-clockwise circulation is found inside the bubble with two clockwise circulations accompanied. A circulation can also be found in the

Case	Experiments		Simulations	
	Experiment conditions	Observed bubble shape	Predicted bubble shape	Modeling conditions
Bubbly	$j_L = 0.2\text{m/s}$ $j_G = 0.1\text{m/s}$			$j_L = 0.24\text{m/s}$ $j_G = 0.09\text{m/s}$
Short slug	$j_L = 0.2\text{m/s}$ $j_G = 0.3\text{m/s}$			$j_L = 0.26\text{m/s}$ $j_G = 0.4\text{m/s}$
Long slug	$j_L = 0.1\text{m/s}$ $j_G = 0.3\text{m/s}$			$j_L = 0.08\text{m/s}$ $j_G = 0.25\text{m/s}$

Fig. 6. Comparison of bubble/slug shapes observed in experiment and simulation.

liquid region. This flow structure is in accordance with the sketch of streamlines given by Taylor (1961) and the experiment by Kashid et al. (2005). However, by using the CSF model, there are four circulations inside the gas bubble. The structure is similar to that shown in Fig. 2 except the direction of circulation due to the external pressure driving force. The fluid inside the bubble is more significantly accelerated because of much lower density of gas phase. The parasitic flow inside the gas bubble also affects the liquid phase and makes the flow disordered. Obviously, these disturbances are not physical. Small Ca number, which results from the dominance of surface tension force, greatly exaggerates the numerical errors in the surface tension formulation and obscures the bulk flow.

The above simulations are repeated under different conditions of pressure gradient and void fraction α . In each simulation, the wall is assumed wetted by liquid in accordance with the experiment of Hayashi et al. (2007). The superficial gas and liquid velocities are $j_G = 0.05\text{--}0.49\text{ m/s}$ and $j_L = 0.055\text{--}0.4\text{ m/s}$, respectively, and the Ca number is $0.0087\text{--}0.27$. Bubble shapes of three typical types, i.e., bubbly, short slug and long slug, are compared in Fig. 6. The bubble keeps nearly a spherical shape due to the strong surface tension force in the case of the bubbly flow. For the short slug flow, with a relative higher liquid velocity, the front part of gas slug is depressed while the rear expanded. With the increase of gas flow rate while decrease of liquid flow rate, the gas slug becomes longer. The strong surface tension force maintains a hemispherical shape at both caps.

Fig. 7 shows the isolines of dimensionless stream function relative to the bubble velocity. The void fraction α is changed as 0.2, 0.5 and 0.6. Anti-clockwise circulation is commonly found in the gas phase for all three cases. The circulation is strong in the region close to wall, where the gas–liquid interface is driven backward by the shear stress. The clockwise circulation present in the front and rear part of long gas bubble. Since the viscous force in the present conditions is weak, these clockwise circulations are greatly depressed compared to the results by Fukagata et al. (2007) with the tube diameter of $20\text{ }\mu\text{m}$. Significant circulations are also found in the liquid slug. These circulations are deemed to enhance the heat transfer as well as increase the pressure drop (Fukagata et al., 2007).

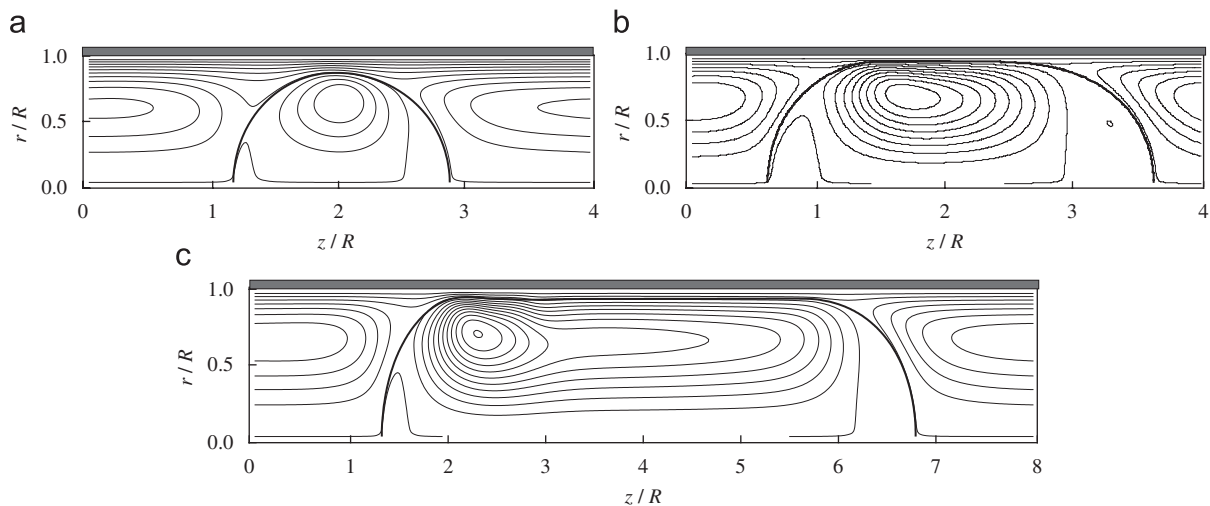


Fig. 7. Bubble shape (bold line) and relative streamlines: (a) bubbly flow; (b) short slug; and (c) long slug.

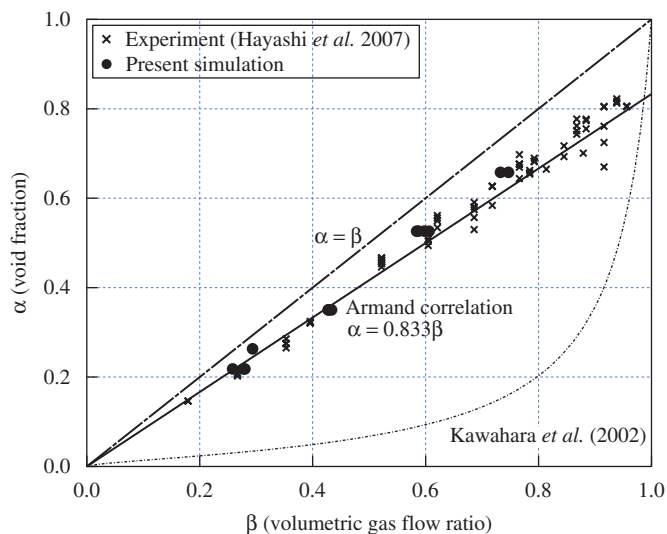


Fig. 8. Relationship between volumetric gas flow ratio (β) and void fraction (α).

Fig. 8 shows the computed relation between the void fraction α and the volumetric gas flow ratio β , which is defined as

$$\beta = \frac{j_G}{j_G + j_L} = \alpha \frac{U_G}{U_{TP}}, \quad U_{TP} = j_G + j_L. \quad (20)$$

The experimental results by Hayashi et al. (2007) are shown in the figure. It is apparent that both experimental and numerical results follow the correlation of Armand, i.e., $\alpha = 0.833\beta$. For higher void fractions,

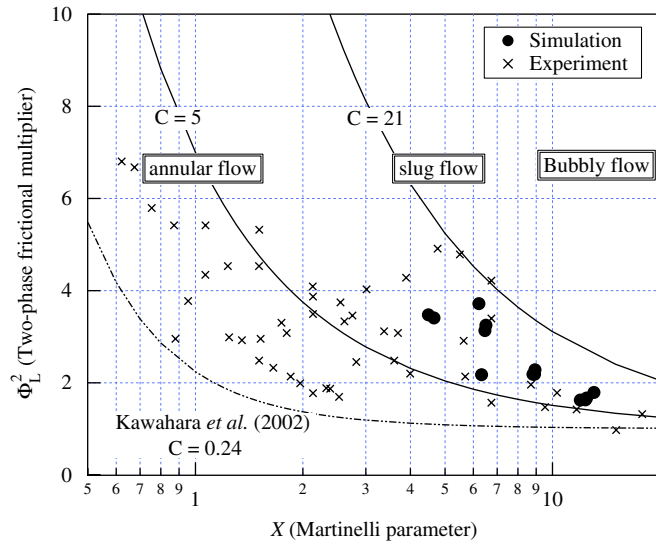


Fig. 9. Lockhart–Martinelli correlation.

the results lie between the Armand correlation and the homogenous model, which is $\alpha = \beta$. Kawahara et al. (2002) proposed a correlation based on the experimental data on a tube of 100 μm in diameter as follows:

$$\alpha = \frac{0.03\beta^{0.5}}{1 - 0.97\beta^{0.5}} \tag{21}$$

In this correlation, β is much larger than α . This may be due to difference in flow conditions; the flow in Kawahara’s (2002) experiment always has a long gas core causing much higher slip velocity. In the present simulate, the gas bubbles are much shorter and the frequency of bubble is higher. Therefore, the flows are much more homogenous.

The Lockhart–Martinelli correlation is a widely used method to represent the pressure drop characteristics for two-phase flow. This correlation uses a two-phase friction multiplier, Φ_L^2 , defined as,

$$\Phi_L^2 = \frac{(-dP/dz)_{TP}}{(-dP/dz)_{LO}} \tag{22}$$

The friction multiplier is correlated in terms of the Lockhart–Martinelli parameter, X , which is given by

$$X^2 = \frac{(-dP/dz)_{LO}}{(-dP/dz)_{GO}} \tag{23}$$

where $(-dP/dz)_{LO}$ and $(-dP/dz)_{GO}$ are the frictional pressure drops when each of liquid and gas alone is assumed to flow in the same tube, respectively. Then, the condition is given as

$$\Phi_L^2 = 1 + \frac{C}{X} + \frac{1}{X^2} \tag{24}$$

where C is a constant ranging from 5 to 21 for macro channels, depending on whether the liquid and gas flows are laminar or turbulent.

Fig. 9 shows the calculated two-phase multiplier and the corresponding experimental ones. The simulated and experimental results are in good agreement in the region of slug and bubbly flow. All the cases are well bounded by two lines of $C = 5$ and 21. Mishima and Hibiki (1996) correlated the experimental results based on tubes of 1–4 mm ID and found that C is smaller than 5 and would decrease with reducing the tube diameter. Kawahara et al. (2002) correlated their pressure drop data and proposed $C = 0.24$ with a 100 μm tube. In accordance with the argument made for Fig. 8, short, but high-frequency gas bubble result in higher pressure drop.

4. Conclusion

Numerical simulation of air–water two-phase flow is carried out under the condition that the surface tension force dominates the flow, i.e., the Ca number is $O(10^{-3})$. To accurately represent surface tension, the surface tension formulations by continuum surface force (CSF) and chemical potential (CP) methods are analyzed and compared. The results show that unbalanced surface tension in the CSF model accelerates the fluid. The resulted parasitic flow component would destroy the flow at a small Ca number. On the other hand, the parasitic flow can be reduced to the level of truncation error by using the CP model because the energy is appropriately transferred between kinetic and surface tension energy.

The method is applied to the simulations of bubbly and slug flows in a micro tube of 600 μm in diameter. The bubble shape and flow patterns are in good agreement with the available experimental and analytical results. The frictional pressure drop is found higher than that proposed by the experimental correlation for tubes of millimeter in diameter. The difference in the bubble length and frequency explains the discrepancy.

Acknowledgments

The authors are grateful to Drs. K. Fukagata (The Keio University), Y. Suzuki and N. Shikazono (The University of Tokyo), for fruitful discussions and comments. This work was supported through the 21st Century COE Program, Mechanical Systems Innovation, by the Ministry of Education, Culture, Sports, Science and Technology of Japan (MEXT).

References

- Anderson, D.M., McFadden, G.B., Wheeler, A.A., 1998. Diffuse-interface methods in fluid mechanics. *Annu. Rev. Fluid Mech.* 30, 139–165.
- Brackbill, J.U., Kothe, D.B., Zemach, C., 1992. A continuum method for modeling surface tension. *J. Comput. Phys.* 100, 335–354.
- Fukagata, K., Kasagi, N., Ua-arayaporn, P., Himeno, T., 2007. Numerical simulation of gas–liquid two-phase flow and convective heat transfer in a micro tube. *Int. J. Heat Fluid Flow*. 28, 72–82.
- Hayashi, S., Kasagi, N., Suzuki, Y., 2007. The effects of inlet flow conditions on gas–liquid two-phase flow in a micro tube. In: 2007 ASME-JSME Therm. Eng. Summer Heat Transfer Conf., Vancouver, Canada.
- Hnat, J.G., Buckmaster, J.D., 1976. Spherical cap bubbles and skirt formation. *Phys. Fluids*. 19, 182–194.

- Jacqmin, D., 1999. Calculation of two-phase Navier–Stokes flows using Phase-Field modeling. *J. Comput. Phys.* 155, 96–127.
- Jamet, D., Torres, D., Brackbill, J.U., 2002. On the theory and computation of surface tension: the elimination of parasitic currents through energy conservation in the second-gradient method. *J. Comput. Phys.* 182, 262–276.
- Kandlikar, S.G., 2002. Fundamental issues related to flow boiling in minichannels and microchannels. *Exp. Therm. Fluid Sci.* 26, 389–407.
- Kashid, M., Gerlach, I., Goetz, S., 2005. Internal circulation within the liquid slugs of a liquid-liquid slug-flow capillary microreactor. *Ind. Eng. Chem. Res.* 44, 5003–5010.
- Kawahara, A., Chung, P.M.-Y., Kawaji, M., 2002. Investigation of two-phase flow pattern, void fraction and pressure drop in a microchannel. *Int. J. Multiphase Flow* 28, 1411–1435.
- Kim, J., 2005. A continuous surface tension force formulation for diffuse-interface models. *J. Comput. Phys.* 204, 784–804.
- Lafaurie, B., Nardone, C., Scardovelli, R., Zaleski, S., Zanetti, G., 1994. Modelling merging and fragmentation in multiphase flows with SURFER. *J. Comput. Phys.* 113, 134–147.
- Mishima, K., Hibiki, T., 1996. Some characteristics of air–water two-phase flow in small diameter vertical tubes. *Int. J. Multiphase Flow* 22, 703–712.
- Meier, M., Yadigaroglu, G., Smith, B.L., 2002. A novel technique for including surface tension in PLIC-VOF methods. *Eur. J. Mech. B/Fluids* 21, 61–73.
- Popinet, S., Zaleski, S., 1999. A front-tracking algorithm for accurate representation of surface tension. *Int. J. Numer. Meth. Fluids* 30, 775–793.
- Shirani, E., Ashgriz, N., Mostaghimi, J., 2005. Interface pressure calculation based on conservation of momentum for front capturing methods. *J. Comput. Phys.* 203, 154–175.
- Sussman, M., Smereka, P., Osher, S., 1994. A level set approach for computing solutions to incompressible two-phase flow. *J. Comput. Phys.* 114, 146–159.
- Taylor, G.I., 1961. Deposition of a viscous fluid on the wall of a tube. *J. Fluid. Mech.* 10, 161–165.
- Tong, A.Y., Wang, Z., 2007. A numerical method for capillarity-dominant free surface flows. *J. Comput. Phys.* 221, 506–523.